



Research paper

Magnetic covalent hybrid of graphitic carbon nitride and graphene oxide as an efficient catalyst support for immobilization of Pd nanoparticles

Samahe Sadjadi^{a,*}, Masoumeh Malmir^b, Majid M. Heravi^{b,*}, Fatemeh Ghoreyshi Kahangi^c^a Gas Conversion Department, Faculty of Petrochemicals, Iran Polymer and Petrochemicals Institute, PO Box 14975-112, Tehran, Iran^b Department of Chemistry, School of Science, Alzahra University, PO Box 1993891176, Vanak, Tehran, Iran^c Department of Chemistry, University Campus 2, University of Gilan, Rasht, Iran

ARTICLE INFO

Keywords:

Graphitic carbon nitride
 Graphene oxide
 Magnetic catalyst
 Coupling reactions
 Pd nanoparticles

ABSTRACT

For the first time a magnetic carbon based hybrid catalyst, Pd@g-C₃N₄-Fe-GO, is prepared through covalent conjugation of magnetic graphitic carbon nitride and graphene oxide followed by incorporation of Pd nanoparticles. First, the formation of the catalyst was confirmed via XRD, TG, BET, TEM, FTIR, ICP and VSM analyses and then its catalytic activity for promoting Suzuki and Sonogashira coupling reactions under mild reaction condition was investigated. To elucidate whether hybridization of two carbon materials could improve the catalytic activity, the catalytic activity of the catalyst was compared with the control catalysts (Pd@g-C₃N₄-GO, Pd@g-C₃N₄-Fe, Pd@Fe-GO, Pd@g-C₃N₄, Pd@GO and the GO/g-C₃N₄ physical hybrid). Moreover, the role of magnetic nanoparticles in the catalytic performance was confirmed. Notably, the catalytic activities of the catalyst and the control sample prepared via physical hybridization of two carbon materials were compared to confirm the effect of covalent conjugation on the catalytic activity. Moreover, the study of the substituent effect of *p*-substituted phenyl iodides was considered by Hammett plot, which revealed a beneficial effect of electron-withdrawing side groups for the C–C coupling reaction. Finally, the recyclability of Pd@g-C₃N₄-Fe-GO as well as leaching of Pd and magnetic nanoparticles was studied.

1. Introduction

Graphitic carbon nitride (g-C₃N₄), the most stable carbon nitride allotrope, is a graphite-like metal-free polymeric carbon nanomaterial containing potent C–N bonds in its layers [1]. To date, g-C₃N₄ has been used in diverse range of applications including (photo) catalysis, detection of hazardous gases, adsorbents, fuel cells, purification of contaminants, etc [2–6]. Despite outstanding thermal and optical properties, g-C₃N₄ suffers from some drawbacks such as low specific surface area, low electronic conductivity and wide band gap [7] that limit its applications in the catalysis.

Graphene that is a two dimensional carbon sheet [8,9] with high surface area, thermal conductivity, chemical stability and mechanical strength is extensively utilized for catalytic purposes [10,11]. However, it is proved that graphene itself exhibits low catalytic activity. Mostly, to improve the catalytic activity of graphene it is hybridized with other materials or chemically modified [7,12,13].

Recently, Qu et al. reviewed the recent advances in the design, synthesis and utility of graphene/graphitic carbon nitride hybrid systems for photo-degradation, O₂ evolution, water splitting etc. [7]. The

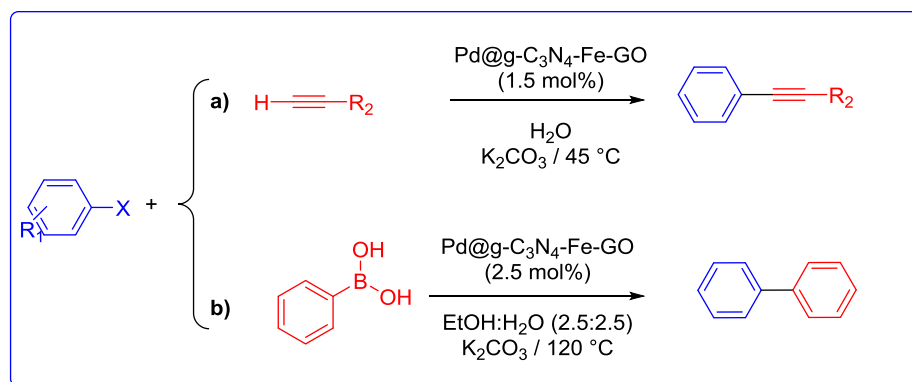
results summarized in that review article confirmed that hybridization of graphene and g-C₃N₄ can be considered as a solution for circumventing the drawbacks of these two carbon materials.

Suzuki and Sonogashira reactions are potent tools for the synthesis of natural products and biologically active organic compounds [14]. These reactions are classically promoted with homogeneous Pd-based catalysts in the presence of phosphine ligand and co-catalyst. Despite all efforts to develop eco-friendly and cost effective protocols for these reactions, tedious work-up, recovery and use of toxic solvents remain as the most challenges [15,16]. To furnish a solution to these issue, use of heterogeneous catalysts has been suggested [17–25].

In the following of our interest in the synthesis of hybrid catalysts contain carbon materials [26–28], herein we wish to report a novel hybrid support, prepared via synthesis and functionalization of g-C₃N₄ followed by incorporation of magnetic nanoparticles (MNPs) and covalent conjugation with GO. The support was then utilized for immobilization of Pd nanoparticles and synthesis of Pd@g-C₃N₄-Fe-GO catalyst. The catalytic activity and recyclability of the catalyst were also studied for Suzuki and Sonogashira reactions (Scheme 1). Moreover, the role of each hybrid component in the catalysis and the effect of

* Corresponding authors.

E-mail addresses: s.sadjadi@ippi.ac.ir (S. Sadjadi), m.heravi@alzahra.ac.ir (M.M. Heravi).



Scheme 1. Model reaction of a) Sonogashira and b) Suzuki coupling reactions.

covalent hybridization was confirmed by comparison of the catalytic activity of Pd@g-C₃N₄-Fe-GO with that of Pd@g-C₃N₄-GO, Pd@g-C₃N₄-Fe, Pd@Fe-GO, Pd@g-C₃N₄, Pd@GO and the GO/g-C₃N₄ physical hybrid. Furthermore, the catalyst recyclability and Pd and Fe leaching were also studied.

2. Experimental section

2.1. Materials and instruments

Pd@g-C₃N₄-Fe-GO was synthesized by using the following reagents and solvents: GO, FeCl₃·6H₂O, FeCl₂·4H₂O, K₂Cr₂O₇, H₂SO₄ ammonia, PdCl₂, urea, thiosemicarbazide, HCl, MeOH, EtOH, NaBH₄, all purchased from Sigma-Aldrich and used as received. To investigate the catalytic activity of Pd@g-C₃N₄-Fe-GO, two types of C–C coupling reactions, i.e. Suzuki and Sonogashira coupling reactions were performed by using acetylene, aryl boronic acid, halobenzene, distilled water and EtOH. All the reagents were of analytical grade and provided from Sigma-Aldrich. Monitoring of the coupling reactions was carried out by using TLC method on commercial aluminum-backed plates of silica gel 60 F254, visualized by using ultraviolet light.

Synthesis of the catalyst was accomplished by using the following apparatus: autoclave of 150 mL and ultrasonic instrument (Bandelin HD 3200 with output power of 150 W and tip TT13). The structure of Pd@g-C₃N₄-Fe-GO was confirmed by using METTLER TOLEDO thermo gravimetric analysis instrument (heating rate of 10 °C min⁻¹, under inert (N₂) atmosphere), PERKIN-ELMER- Spectrum 65 instrument, ICP analyzer (Varian, Vista-pro), CM30300Kv field emission transmission electron microscope, Siemens D5000 (for XRD analysis), vibrating sample magnetometer (VSM, Lakeshore 7407) at room temperature and BELSORP Mini II instrument (degassing of the sample for 3 h at 423 K).

2.2. Catalyst preparation

2.2.1. Synthesis of porous g-C₃N₄ nano sheet: g-C₃N₄-OX

Initially, the g-C₃N₄ nano-sheet was prepared through urea pyrolysis [26,27]. Typically, 10 g of urea was grounded into powder, then heated and calcined at 450 °C for 4.5 h with a heating rate of 1.6 °C/min. The resulting light yellow product was then oxidized via the chemical oxidation with K₂Cr₂O₇/H₂SO₄. In detail, 1 g of the g-C₃N₄ nano sheet was dissolved in the solution of K₂Cr₂O₇ (20 g in 100 mL of H₂SO₄) and then stirred thoroughly for 2 h at room temperature. Next, the mixture was slowly poured into 400 mL of deionized water and cooled to room temperature. After centrifugation at 10000 rpm, the resulting light yellow solid was dialyzed in a dialysis bag to remove all residual acids, and dispersed in water for 1 h. Finally, the obtained cream suspension 1 was dried at 80 °C overnight.

2.2.2. Preparation of MNPs

MNPs were prepared according to the previously reported procedure [29–31]. Typically, FeCl₃·6H₂O (20 mmol) and FeCl₂·4H₂O (10 mmol) were dissolved in 100 mL of distilled water into a two-necked round-bottom flask (250 mL) and heated at 90 °C under N₂ atmosphere for 1 h. Then, a solution of concentrated aqueous ammonia (10 mL) was added into a solution. After cooling, the resulting magnetic particles 2 was collected by using an external magnet, washed with distilled water and dried in a vacuum oven at 60 °C for 12 h.

2.2.3. Synthesis of magnetic g-C₃N₄

In order to synthesize magnetic porous g-C₃N₄ nano sheet, Fe₃O₄ (1 g) was suspended in a 50 mL of HCl solution (6 M). Then, the resulting mixture was sonicated at ambient temperature. The temperature of the reaction mixture was kept constant by using icy water bath. After 0.5 h, g-C₃N₄ (1 g) was introduced into the mixture and the resulting suspension was sonicated for further 1 h. Then, the reaction mixture was transferred to the 150 mL autoclave and heated at 220 °C overnight. Upon completion of the hydrothermal process, the as-prepared 3 was collected magnetically, washed several times with EtOH/H₂O and dried at 80 °C for 12 h in oven.

2.2.4. Synthesis of amine functionalized magnetic g-C₃N₄

The amine functionalized magnetic g-C₃N₄ was obtained by dissolving thiosemicarbazide (0.8 g) in the stirring suspension of magnetic g-C₃N₄ (1.5 g) in MeOH (50 mL) followed by refluxing overnight. Upon completion, the resulting solid was filtered off, washed with hot MeOH repeatedly and dried at 100 °C overnight.

2.2.5. Hybridization of magnetic g-C₃N₄ with graphene oxide: Synthesis of g-C₃N₄-Fe-GO

The reaction mixture was formed by adding dispersed magnetic g-C₃N₄ nano sheet (1.3 g in 25 mL water) into GO solution (0.7 g in 25 mL water) under sonication. After sonicating the mixture for 20 min, it was heated to 90 °C and stirred for 6 h vigorously. Upon completion of the reaction, the resultant solid was separated magnetically, washed with hot EtOH repeatedly and dried at 60 °C overnight.

2.2.6. Immobilization of Pd NPs on the g-C₃N₄-Fe-GO: Pd@g-C₃N₄-Fe-GO

To immobilize Pd nanoparticles on g-C₃N₄-Fe-GO, g-C₃N₄-Fe-GO (1.5 g) was dispersed in EtOH (40 mL) by sonication for 0.5 h. Then, a solution of PdCl₂ (0.15 g) in 10 mL deionized water was added into the suspension under stirring condition overnight. Subsequently, a solution of NaBH₄ (0.2 M, 10 mL) was added into the mixture in a drop wise manner. Subsequently, the resulting mixture was stirred for 3 h. Then, the product 5 was magnetically collected, washed with MeOH/H₂O for three times and dried at 60 °C for 12 h (Fig. 1).

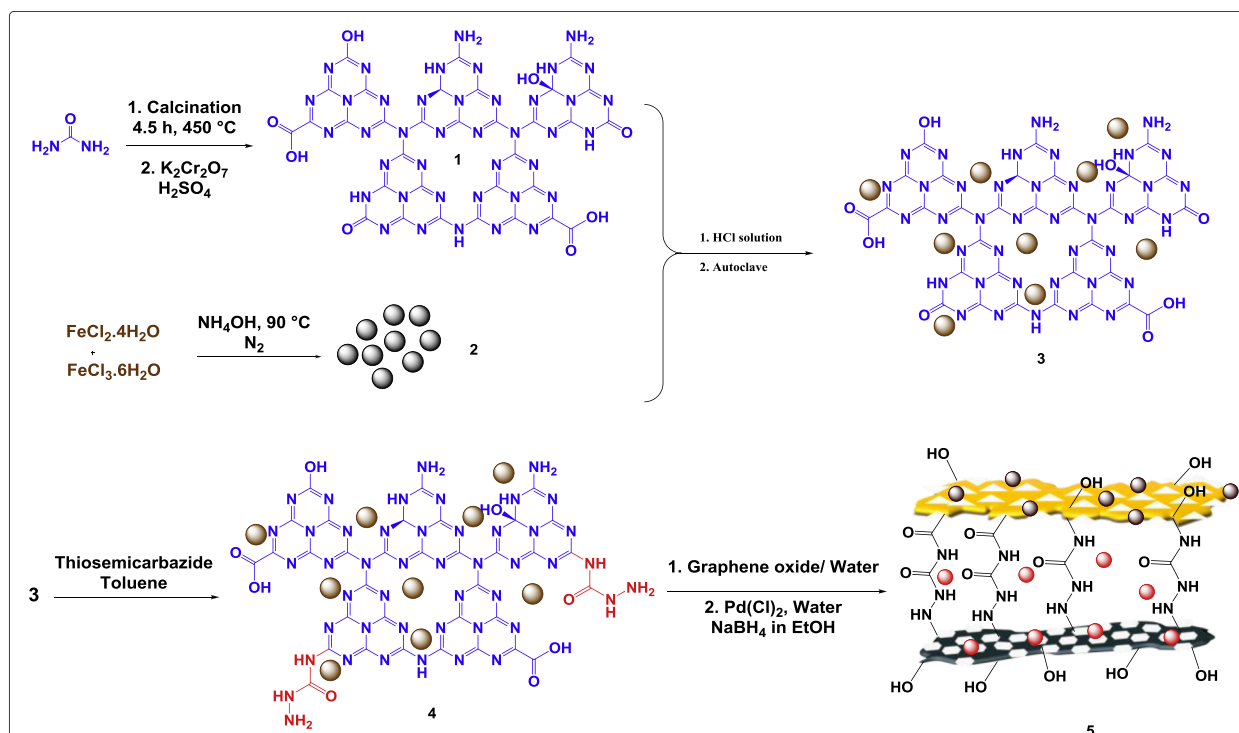


Fig. 1. The procedure for the synthesis of Pd@g-C₃N₄-Fe-GO.

2.3. C-C coupling reactions

2.3.1. Typical procedure for Sonogashira reaction

Halobenzene (1.0 mmol), acetylene (1.0 mmol), Pd@g-C₃N₄-Fe-GO (1.5 mol%) and K₂CO₃ (2.0 mmol in 5.0 mL water) as a base were mixed in water (5.0 mL). The resulting mixture was then heated at 45 °C for appropriate reaction time. Upon completion of the reaction (traced by TLC, ratio of *n*-hexane/ethyl acetate: 8/2), Pd@g-C₃N₄-Fe-GO was collected magnetically, washed with EtOH three times and dried in oven at 100 °C overnight. On the other hand, the filtrate, was cooled to room temperature and the organic layer was extracted with diethyl ether (10 mL). The resulting coupling product was purified by column chromatography over silica gel (Scheme 1a).

2.3.2. Typical procedure for Suzuki reaction

Aryl halide (1.0 mmol) and aryl boronic acid (1.2 mmol) were mixed and dissolved in water/EtOH (2.5:2.5, 10 mL) and then K₂CO₃ (2.0 mmol) and Pd@g-C₃N₄-Fe-GO (2.5 mol %) were added into a mixture. The flask containing reaction mixture was then placed in an oil bath (120 °C) and stirred for appropriate time. At the end of the reaction (traced by TLC, ratio of *n*-hexane/ethyl acetate: 7/3), the mixture was cooled to room temperature and the catalyst was separated magnetically and washed with EtOH three times and dried in oven at 100 °C overnight. Finally, the solvent was removed under reduced pressure and the product was extracted with hexane (10 mL). The resulting coupling product was purified by column chromatography over silica gel (Scheme 1b).

3. Result and discussion

3.1. Catalyst characterization

To verify the formation of the catalyst, it was subjected to various analyses. First, the FTIR spectrum of Pd@g-C₃N₄-Fe-GO was recorded and compared with the spectra of GO, g-C₃N₄, MNPs and g-C₃N₄.OX. As illustrated in Fig. 2, the FTIR spectrum of g-C₃N₄ is in a good

accordance with the previous reports and shows the characteristic bands [32] at 3000–3392 cm⁻¹ (N–H and O–H groups) and 1247–1633 cm⁻¹ (C–N group). In the FTIR spectrum of g-C₃N₄.OX, not only the characteristic bands of g-C₃N₄ can be observed, but also an additional band at 1691 cm⁻¹ is detectable that can be due to the –C=O functionalities. As illustrated, the characteristic bands of MNPs are appeared at 1620 cm⁻¹, 3424 cm⁻¹, 633 cm⁻¹ and 599 cm⁻¹. The FTIR spectrum of GO exhibited the bands at 1622 cm⁻¹, 1711 cm⁻¹, 3418 cm⁻¹ and 1041 cm⁻¹. The FTIR spectrum of the catalyst exhibited the characteristic bands of MNPs, g-C₃N₄ and GO. Notably, as the most of the characteristic bands of these components overlapped, FTIR solely cannot confirm the formation of the catalyst.

In Fig. 3, the thermograms of GO, g-C₃N₄ and the catalyst are depicted. The observed mass loss in the thermogram of g-C₃N₄ (at ~670 °C) can be attributed to the degradation of g-C₃N₄ sheet [33]. In the thermogram of GO a mass loss can be detected at ~170 °C that can be assigned to the detachment of oxygen-containing functional groups from the surface of GO. Comparing the thermogram of the catalyst with that of GO and g-C₃N₄, it can be concluded that the thermal stability of the catalyst is higher than GO and lower than g-C₃N₄. More precisely, two mass losses can be observed in the thermogram of the catalyst, the first one, observed at ~175 °C is due to the detachment of oxygen-containing functional groups from the surface of GO and the next one, occurred at 590 °C, is stemmed from g-C₃N₄ degradation.

In Fig. 4 the XRD pattern of the catalyst is illustrated. As depicted, a broad halo can be observed at 2θ = 17–27 that is representative of the g-C₃N₄. Moreover, the observed peaks at 40°, 46.4°, 69.2° and 81° (JCPDS, Card No. 46-1043) can also be assigned to Pd nanoparticles [34]. According to the literature, the XRD pattern exhibit the characteristic peaks of hematite (ICDD Card NO. 33-0664) [35,36]. The peaks appearing at 2θ range of 24.1°, 33.1°, 36°, 40.7°, 50.2°, 54.1°, 57.42°, 64.3° and 65.7° can be attributed to the 012, 104, 110, 113, 024, 116, 018, 214 and 300 crystalline structures corresponding to pure α-Fe₂O₃ nanoparticles [35,36].

Notably, in the XRD pattern of the catalyst, the characteristic peaks of GO (Fig. S1) at 2θ = 10.5° and 42.4° were not observed. This can be

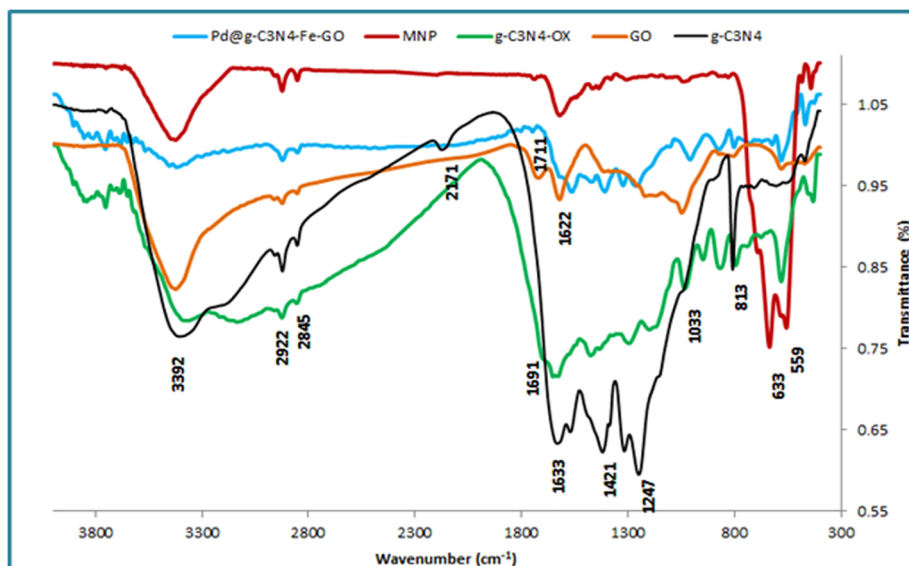


Fig. 2. The FTIR spectra of MnPs, GO, g-C₃N₄, g-C₃N₄-OX and Pd@g-C₃N₄-Fe-GO.

attributed to the reduction of GO in the course of the preparation process [37].

Metal loading of Pd@g-C₃N₄-Fe-GO was also measured via ICP analysis. In this line, sample preparation was performed according to the literature [26] and ICP analysis was carried out for measuring Fe and Pd atoms. Following this method, the contents of Fe and Pd was estimated to be 6 and 1 wt% respectively.

To study the magnetic feature of Pd@g-C₃N₄-Fe-GO, room temperature vibrating sample magnetometer (VSM) was applied and the maximum saturation magnetization (*M_s*) value of the catalyst was estimated and compared with that of bare magnetic nanoparticle. The results showed that the *M_s* value of Pd@g-C₃N₄-Fe-GO (31.15 emu g⁻¹) is lower than that of bare magnetic nanoparticle (47 emu g⁻¹), Fig. 5.

In Fig. 6 the TEM images of g-C₃N₄-Fe-GO and Pd@g-C₃N₄-Fe-GO are illustrated. As shown, in the TEM image of g-C₃N₄-Fe-GO the g-C₃N₄ sheet can be detected. Moreover, MnPs can be observed as black spots on the g-C₃N₄ sheet. In the case of Pd@g-C₃N₄-Fe-GO (Fig. 6B), apart from the fine g-C₃N₄ sheet, the GO sheet can be observed as darker sheet.

Further characterization of Pd@g-C₃N₄-Fe-GO was carried out by performing BET analysis. The nitrogen adsorption–desorption isotherm of the catalyst, Fig. S2, showed type IV isotherms [38] with H3 hysteresis loops [39]. Using BET data, the specific surface area of the catalyst was estimated to be 35 m²g⁻¹ that is lower than that of GO (150 m²g⁻¹) and almost similar to that of g-C₃N₄ (36 m²g⁻¹).

3.2. Catalytic activity

Initially, to optimize the reaction conditions, two model Suzuki and Sonogashira reactions, reaction of benzyl iodide and boronic acid and reaction of phenyl acetylene and benzyl iodide, were selected. Then, the reaction conditions were optimized by varying the reaction variables, i.e., reaction temperature, solvent, the required amount of the catalyst and type of the base (Table S1). Upon disclosing the optimum reaction condition, it was studied whether hybridization of GO with g-C₃N₄ and incorporation of MnPs could improve the catalytic activity. To this purpose, several control catalysts were prepared and their catalytic activity for the model coupling reactions were compared with that of

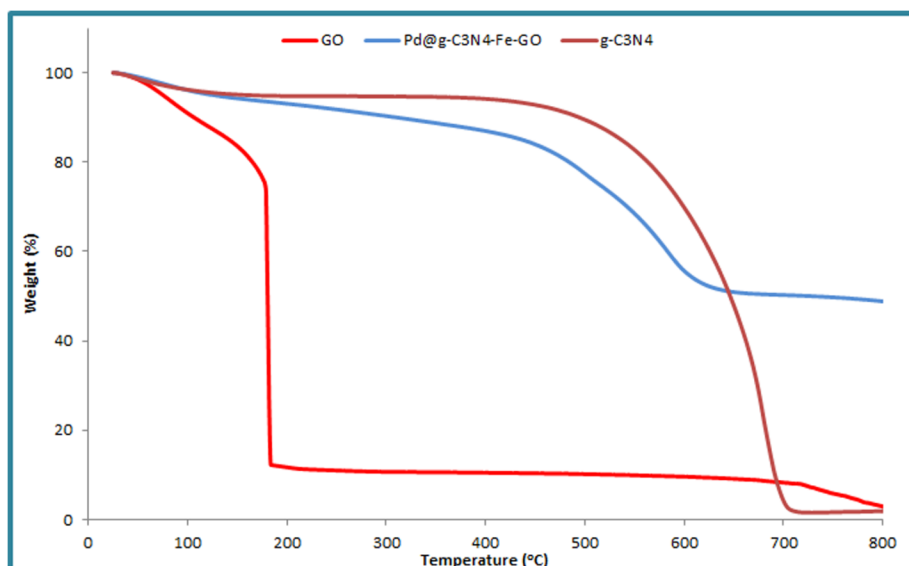


Fig. 3. The TG analyses of the g-C₃N₄, GO and Pd@g-C₃N₄-Fe-GO.

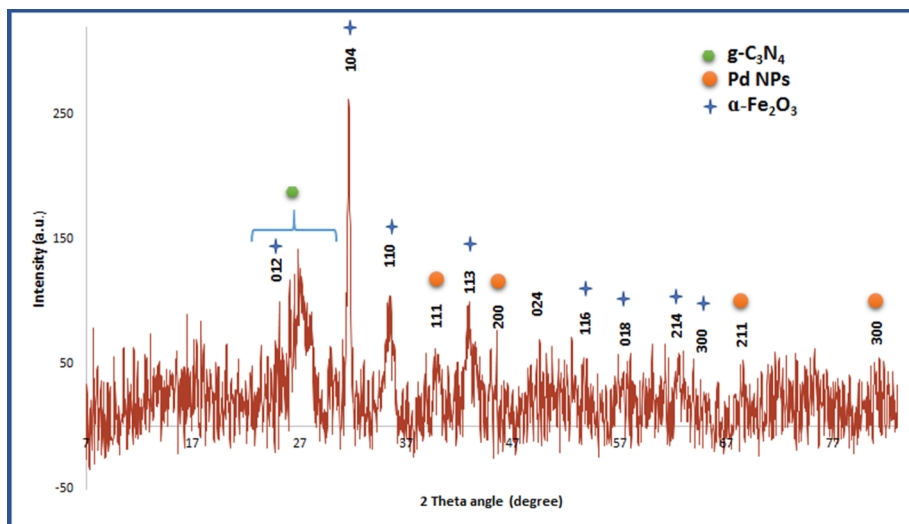


Fig. 4. The XRD analysis of the Pd@g-C₃N₄-Fe-GO.

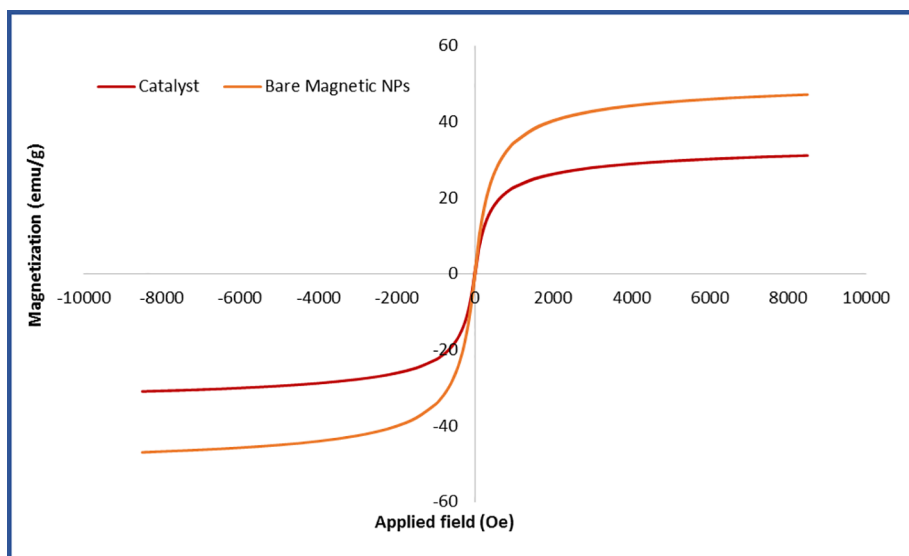


Fig. 5. The VSM analyses of the bare magnetic NPs and Pd@g-C₃N₄-Fe-GO catalyst.

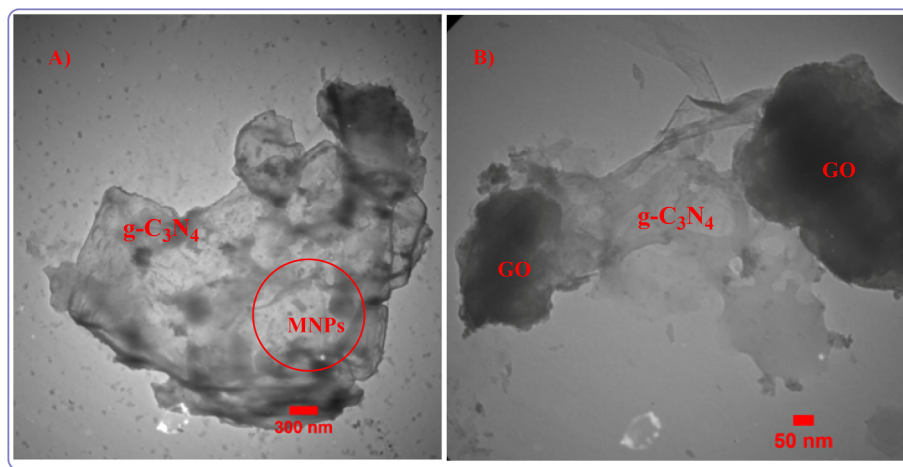


Fig. 6. The TEM images of the g-C₃N₄-Fe-GO (A) and Pd@g-C₃N₄-Fe-GO (B).

Table 1

Comparison of the catalytic activity of the present catalyst with the other prepared catalysts in the coupling reactions.

Entry	Catalyst	Sonogashira coupling reaction ^a			Suzuki coupling reaction ^b		
		Yield ^g (%)	Time (min)	TOF (h ⁻¹)	Yield ^h (%)	Time (min)	TOF (h ⁻¹)
1	Pd@g-C ₃ N ₄ -Fe-GO	92	70	5287	94	120	1880
2	Pd@g-C ₃ N ₄ -GO ^c	85	70	4885	80	120	1600
3	Pd@g-C ₃ N ₄ -Fe-GO ^d	50	70	2873	68	120	1360
4	Pd@Fe-GO ^e	60	70	3448	55	120	1100
5	Pd@g-C ₃ N ₄ -Fe ^f	75	70	4310	75	120	1500
6	Pd@g-C ₃ N ₄	40	180	888	50	180	666
7	Pd@GO	30	180	666	45	180	600

^a Reaction condition: aryl halide (1.0 mmol), terminal alkyne (1.2 mmol), catalyst (1.5 mol%), K₂CO₃ (2.0 mmol) in water (5.0 mL) at 45 °C.^b Reaction condition: aryl halide (1.0 mmol), boronic acid (1.2 mmol), Pd@g-C₃N₄-Fe-GO (2.5 mol%), K₂CO₃ (2.0 mmol) in water:EtOH (2.5:2.5, 10 mL) at 120 °C.^c Non-magnetic catalyst (without Fe₂O₃).^d Without thiosemicarbazide.^e Palladium catalyst without g-C₃N₄.^f Palladium catalyst without GO.^g Isolated yield.^h Isolated yield.**Table 2**Pd@g-C₃N₄-Fe-GO catalyzed Sonogashira reaction of various halides with terminal alkynes.^a

Entry	X	R ¹	R ²	Time (min)	Yield (%)	TOF (h ⁻¹)
1	I	H	Ph	70	92	5287
2	I	<i>p</i> -Me	Ph	255	80	1254
3	I	<i>p</i> -OMe	Ph	195	90	1846
4	I	<i>p</i> -COMe	Ph	220	80	1457
5	I	<i>p</i> -NO ₂	Ph	195	85	1743
6	I	1-naphthalene	Ph	120	85	2833
7	I	H	CH ₂ OH	90	95	4222
8	I	<i>p</i> -OMe	CH ₂ OH	90	95	4222
9	I	<i>p</i> -Me	CH ₂ OH	120	95	3166
10	I	<i>p</i> -COMe	CH ₂ OH	115	80	2792
11	I	<i>p</i> -NO ₂	CH ₂ OH	75	90	4800
12	I	1-naphthalene	CH ₂ OH	100	88	3534
13	Br	H	Ph	135	73	2162
14	Cl	H	Ph	165	65	1575

Pd@g-C₃N₄-Fe-GO catalyzed Suzuki-Miyaura reaction of various halides with terminal alkynes^b

15	I	H	120	94	1880
16	I	<i>p</i> -Me	160	80	1130
17	I	<i>p</i> -OMe	140	86	1476
18	I	<i>p</i> -CO ₂ Me	135	92	1635
19	I	<i>p</i> -NO ₂	120	90	1800
20	I	1-naphthalene	180	85	1133
21	Br	H	280	82	703
22	Cl	H	330	80	581

^a Reaction condition: aryl halide (1.0 mmol), terminal alkyne (1.2 mmol), Pd@g-C₃N₄-Fe-GO (1.5 mol%), K₂CO₃ (2.0 mmol) in water (5.0 mL) at 45 °C.^b Reaction condition: aryl halide (1.0 mmol), boronic acid (1.2 mmol), Pd@g-C₃N₄-Fe-GO (2.5 mol%), K₂CO₃ (2.0 mmol) in water:EtOH (2.5:2.5, 10 mL) at 120 °C.Pd@g-C₃N₄-Fe-GO, [Table 1](#).

First, Pd@Fe-GO and Pd@g-C₃N₄ were prepared (see SI) and their catalytic activities for both Sonogashira and Suzuki model reactions were studied. As tabulated in [Table 1](#), the yields of the model products was lower than that of Pd@g-C₃N₄-Fe-GO, indicating that hybridization of GO and g-C₃N₄ could effectively improve the catalytic activity. The incorporation of GO can improve the specific surface area of the catalyst. In other word, the specific surface area of g-C₃N₄ (with no metal loading) was 36 m²g⁻¹ that can be significantly reduced upon incorporation of Fe and Pd nanoparticles. However, in the hybrid system of g-C₃N₄ and Go, the specific surface area of the catalyst after metal loading was measured to be 35 m²g⁻¹. This indicate the role of GO in enhancing the specific surface area. Moreover, it can be assume

that the unpaired electrons on the GO can facilitate electron transfer to metal or other active centers [40].

Then, the contribution of MNPs in the catalysis was investigated. In this line, Pd@g-C₃N₄-GO was prepared and applied as a catalyst for the model coupling reactions. The comparison of the catalytic activity of Pd@g-C₃N₄-Fe-GO with Pd@g-C₃N₄-GO confirmed that MNPs could improve the catalytic activity to some extent. Notably, the main role of MNPs is in catalyst recovery. Notably, it can be assumed that the interaction between Pd and Fe may affected the surface diffusion of Pd atoms during immobilization, which led to the formation of fine hybrid system [41].

Next, it was investigated whether the covalent conjugation of GO and g-C₃N₄ could affect the catalytic activity. To this purpose, a control catalyst Pd@g-C₃N₄-Fe-GO^o was prepared through immobilization of Pd nanoparticles on the physical hybrid of g-C₃N₄ and GO (see SI). Interestingly, this control catalyst exhibited lower catalytic activity compared to Pd@g-C₃N₄-Fe-GO, implying the remarkable role of covalent conjugation of Go and g-C₃N₄ in the catalysis.

Confirming the role of each component of the hybrid system in the catalysis, the scope of the developed protocols for Sonogashira and Suzuki coupling reaction was studied by synthesis of various coupling derivatives, [Table 2](#). As illustrated, Pd@g-C₃N₄-Fe-GO could promote the reaction of various substrates with different electronic and steric features and furnish the corresponding products in high yields. As expected, the less active aryl halides, i.e. aryl chlorides and aryl bromides led to the corresponding products in longer reaction times and lower yields. Moreover, use of aryl halides with electron withdrawing groups was more successful and higher yields of products were achieved. Notably, the steric substrates, 1-naphthalene, could also tolerated the reaction to afford the corresponding product in 85% yield.

We further obtained a Hammett plot to measure quantitatively the effects of electronic changes in phenyl iodide on the rates of Sonogashira and Heck reaction. The relative rates of coupling of *p*-substituted phenyl iodide (*p*-H, *p*-NO₂, *p*-Me, *p*-OMe) were investigated. A linear relationship was found between log (k_x/k_H) and σ_p – ([Figs. 7 and 8](#)). The slope of the plots show reaction constant ρ values of 0.33 and 0.27 for the studied phenyl iodide derivatives for Sonogashira and Heck coupling reactions. These results suggest development of a negative charge at the reaction center.

3.3. Catalyst recyclability

Considering the importance of recyclability of heterogeneous catalysts from the industrial point of view, the recyclability of Pd@g-C₃N₄-Fe-GO for both Suzuki and Sonogashira model reactions were

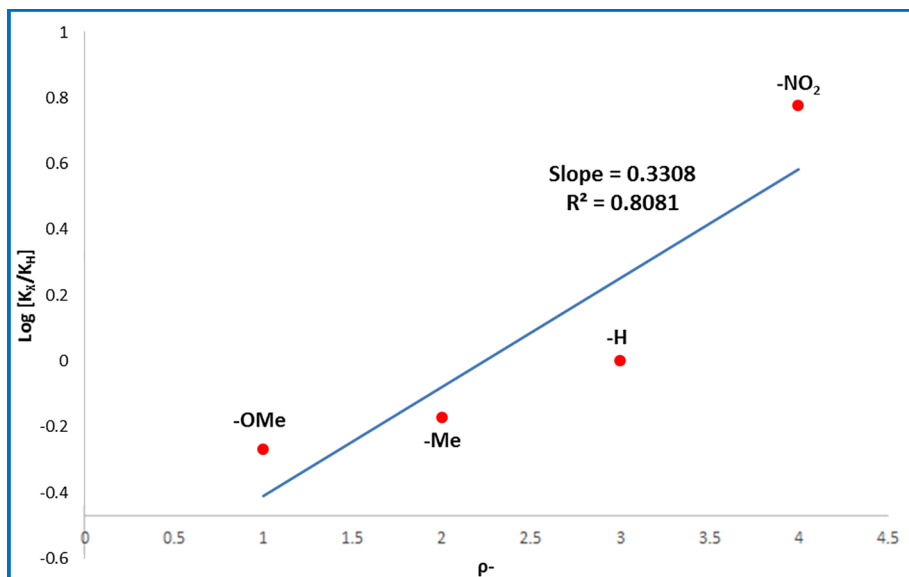


Fig. 7. The Hammett plot for the competitive couplings of *p*-substituted phenyl iodide with phenyl acetylene.

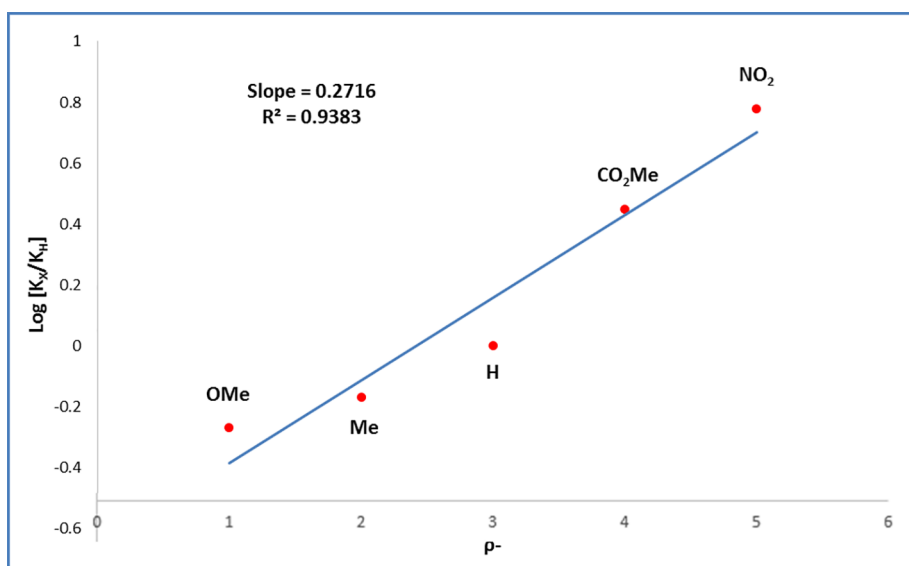


Fig. 8. The Hammett plot for the competitive couplings of *p*-substituted phenyl iodides with boronic acid.

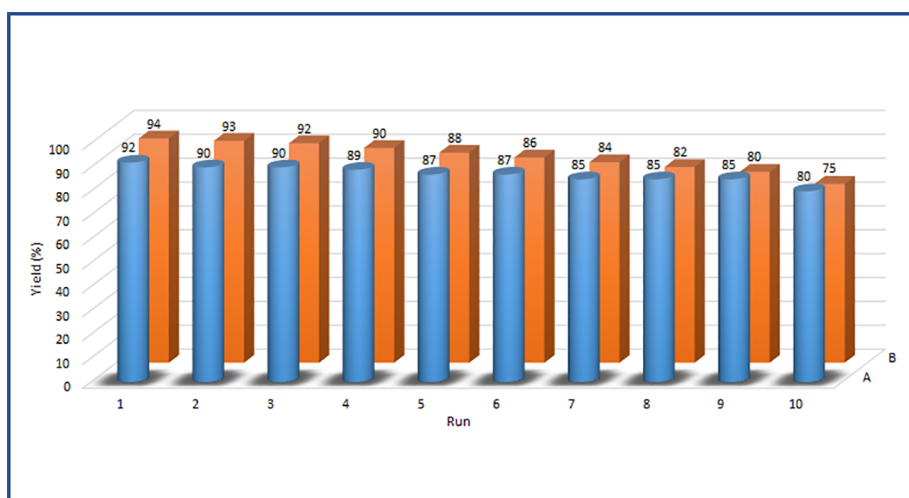


Fig. 9. Recyclability of the Pd@g-C₃N₄-Fe-GO in the A) Sonogashira and B) Suzuki coupling reactions.

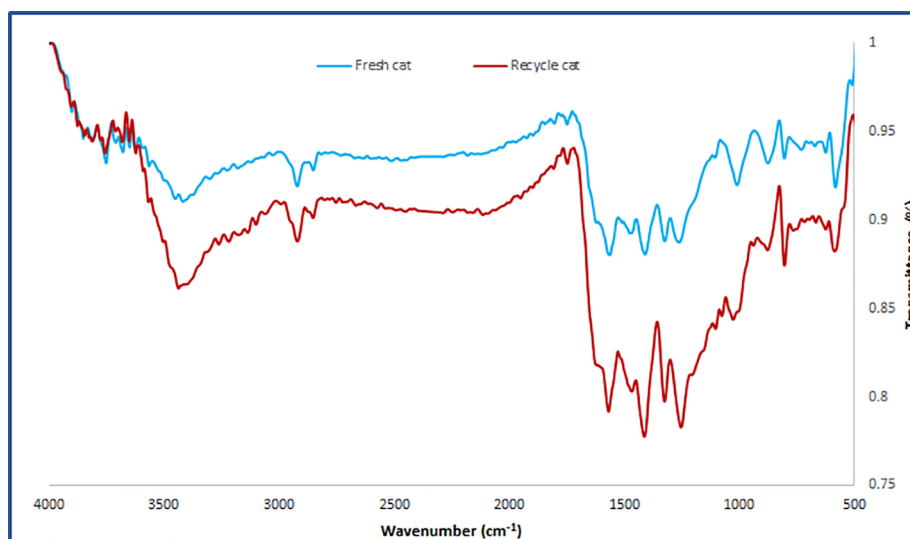


Fig. 10. The FTIR spectra of fresh and recycled Pd@g-C₃N₄-Fe-GO.

investigated. As described in the experimental section, at the end of the reaction, the catalyst was magnetically separated from the reaction mixture, washed, dried and subjected to the next run of the model reactions under exactly similar reaction condition. After each reaction runs, the yield of the model coupling product was estimated and compared with that of the fresh Pd@g-C₃N₄-Fe-GO. The comparison of the yield of fresh and recycled catalysts, Fig. 8, confirmed high recyclability of the catalyst. As depicted in Fig. 9, the recyclability of the catalyst for Sonogashira reaction was slightly higher than Suzuki coupling reaction. More precisely, only 12% loss of the catalytic activity was observed for Sonogashira reaction, while the yield of the Suzuki model product showed 19% decrease upon recycling for 10 times.

To further study the recycled catalyst, it was subjected to the FTIR spectroscopy. The comparison of the FTIR spectrum of the fresh and recycled catalyst after 10 Sonogashira reaction time, Fig. 10, confirmed that Pd@g-C₃N₄-Fe-GO was structurally stable in the course of recycling and the FTIR spectrum of the recycled catalyst contained the characteristic bands of the fresh ones.

Finally, the leaching of both Pd and Fe atoms were measured by using ICP analysis. The results indicated low leaching of the two metals upon catalyst recycling. Notably, up to the tenth recycling run, the catalyst preserved its magnetic property and could be recovered by using external magnet. Notably, using TEM analysis, the average diameter size of Pd nanoparticles after the reaction was calculated to be ~8.7 nm, slightly larger than that of the as-prepared catalyst (8 nm).

4. Conclusion

In conclusion, a novel magnetic covalent hybrid of GO and g-C₃N₄ was prepared via oxidation and subsequent functionalization of g-C₃N₄ followed by incorporation of MNPs and covalent conjugation with GO. The prepared hybrid, g-C₃N₄-Fe-GO, was then used for immobilization of Pd nanoparticles. The furnished compound, Pd@g-C₃N₄-Fe-GO, was then applied as a heterogeneous catalyst for promoting Sonogashira and Suzuki coupling reactions under mild reaction conditions. Precise studies using control samples confirmed the contribution all hybrid components in the catalysis. Moreover, it was proved that hybridization of GO and g-C₃N₄ could improve the catalytic activity. Notably, the covalent conjugation was significantly more effective than physical mixture. The catalyst recyclability tests also confirmed the high recyclability of the catalyst and low Pd and Fe leaching.

Acknowledgements

The authors appreciate partial financial supports from Iran Polymer and Petrochemical Institute and Alzahra University.

Appendix A. Supplementary data

Supplementary data to this article can be found online at <https://doi.org/10.1016/j.ica.2018.12.048>.

References

- [1] J. Liu, H. Wang, M. Antonietti, *Chem Soc Rev.* 45 (2016) 2308–2326.
- [2] Y. Gong, M. Li, H. Li, Y. Wang, *Green Chem.* 17 (2015) 715–736.
- [3] A. Wang, C. Wang, L. Fu, W. Wong-Ng, Y. Lan, *Nano-Micro Lett.* 47 (2017) 1–22.
- [4] T. Ye, D.P. Durkin, N.A. Banek, M.J. Wagner, D. Shuai, *A.C.S. Appl. Mater. Interfaces* 9 (2017) 27421–27426.
- [5] Y. Wang, X. Bai, H. Qin, F. Wang, Y. Li, X. Li, S. Kang, Y. Zuo, L. Cui, *A.C.S. Appl. Mater. Interfaces* 8 (2016) 17212–17219.
- [6] S. Elavarasan, B. Baskar, C. Senthil, P. Bhanja, A. Bhaumik, P. Selvam, M. Sasidharan, *RSC Adv.* 6 (2016) 49376–49386.
- [7] Q. Han, N. Chen, J. Zhang, L. Qu, *Mater. Horiz.* 4 (2017) 832–850.
- [8] B. Qiu, M. Xing, Z. J., *Chem. Soc. Rev.* 47 (2018) 2165–2216.
- [9] C. Huang, C. Li, G. Shi, *Energy Environ. Sci.* 5 (2012) 8848–8868.
- [10] W. Song, Z. Chen, C. Yang, Z. Yang, J. Tai, Y. Nan, H. Hongbin Lu, *J. Mater. Chem. A* 3 (2015) 1049–1057.
- [11] Q. Yao, Z.-H. Lu, W. Huang, X. Chen, J. Zhu, *J. Mater. Chem. A* 4 (2016) 8579–8583.
- [12] F. Fliu, F. Niu, T. Chen, J. iHan, Z. Liu, W. Yang, Y. Xu, J. Liu, *Carbon* 134 (2018) 316–325.
- [13] B. Sakthivel, D.S.R. RubyJosephin, K. Sethuraman, A. Dhakshinamoorthy, *Catal. Commun.* 108 (2018) 41–45.
- [14] B.-N. Lin, S.-H. Huang, W.-Y. Wu, C.-Y. Mou, F.-Y. Tsai, *Molecules* 15 (2010) 9157–9173.
- [15] A.R. Hajipour, Z. Shirdashtzade, G. Azizi, *Appl. Organometal. Chem.* 28 (2014) 696–698.
- [16] R. Chinchilla, C. Nájera, *Chem. Soc. Rev.* 40 (2011) 5084–5121.
- [17] M. Bakherad, *Appl. Organomet. Chem.* 27 (2013) 125–140.
- [18] M. Bakherad, R. Doosti, M. Mirzaee, K. Jadidi, *Tetrahedron* 73 (2017) 3281–3287.
- [19] P.V. Rathod, V.H. Jadhav, *Tetrahedron Lett.* 58 (2017) 1006–1009.
- [20] M. Esmailpour, A. Sardarian, J. Javidi, *Catal. Sci. Technol.* 6 (2016) 4005–4019.
- [21] M. Nasrollahzadeh, S.M. Sajadi, M. Maham, A. Ehsani, *RSC Adv.* 5 (2015) 2562–2567.
- [22] R. Zhou, W. Wang, Z.-J. Jiang, H.-Y. Fu, X.-L. Zheng, C.-C. Zhang, H. Chen, R.-X. Li, *Catal. Sci. Technol.* 4 (2014) 746–751.
- [23] M. Nasrollahzadeh, M. Khalaj, A. Ehsani, *Tetrahedron. Lett.* 55 (2014) 5298–5301.
- [24] M. Shunmughanathan, P. Puthiaraj, K. Pitchumani, *Chem. Cat. Chem.* 7 (2015) 666–673.
- [25] A.S. Roy, J. Mondal, B. Banerjee, P. Mondal, A. Bhaumik, S. Manirul Islam, *Appl. Catal., A* 469 (2014) 320–327.
- [26] S. Sadjadi, N. Bahri-Laleh, *J. Porous Mater.* 25 (2018) 821–833.
- [27] S. Sadjadi, M. Malmir, M.M. Heravi, *Appl. Organomet. Chem.* 32 (2018) e4413.

- [28] S. Sadjadi, M.M. Heravi, M. Raja, *Carbohydr. Polym.* 185 (2018) 48–55.
- [29] E. Rafiee, S. Eavani, *Green Chem.* 13 (2011) 2116–2122.
- [30] F. Nemati, R.S. Rad, *Chin. Chem. Lett.* 24 (2013) 370–372.
- [31] F. Nemati, M.M. Heravi, R.S. Rad, *Chin. J. Catal.* 33 (2012) 1825–1831.
- [32] S.C. Yan, Z.S. Li, Z.G. Zou, *Langmuir* 25 (2009) 10397–10401.
- [33] K.C. Christoforidis, M. Melchionna, T. Montini, D. Papoulis, E. Stathatos, S. Zafeiratos, E. Kordouli, P. Fornasiero, *RSC Adv.* 6 (2016) 86617–86626.
- [34] D. Hao, S. Xue-Zhao, S. Cheng-Min, H. Chao, X. Zhi-Chuan, L. Chen, T. Yuan, W. Deng-K, G. Hong-Jun, *Chin. Phys. B* 19 (2010) 106104–106101 106105.
- [35] J. Hua, J. Gengsheng, *Mater. Lett.* 63 (2009) 2725–2727.
- [36] T. Almeida, M. Fay, Y.Q. Zhu, P.D. Brown, *J. Phys. Chem. C* 113 (2009) 18689–18698.
- [37] G. Li, R. Deng, G. Peng, C. Yang, Q. He, Y. Lu, H. Shi, *Water Sci Technol.* 77 (2018) 2220–2227.
- [38] T. Di, B. Zhu, B. Cheng, J. Yu, J. Xu, *J. Catal.* 352 (2017) 532–541.
- [39] P. Yuan, P.D. Southon, Z. Liu, M.E.R. Green, J.M. Hook, S.J. Antill, C.J. Kepert, *J. Phys. Chem. C* 112 (2008) 15742–15751.
- [40] K. Jasuja, J. Linn, S. Melton, V. Berry, *J. Phys. Chem. Lett.* 1 (2010) 1853–1860.
- [41] Z. Zhang, C. Zhang, J. Sun, T. Kou, Q. Bai, Y. Wang, Y. Ding, *J. Mater. Chem. A* 1 (2013) 3620–3628.